Heliyon 10 (2024) e25083

Contents lists available at ScienceDirect

Heliyon

journal homepage: www.cell.com/heliyon

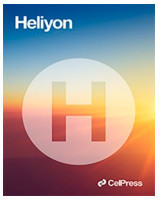

Research article

Genomic insight into *O*-demethylation of 4-methoxybenzoate by a two-component system from *Amycolatopsis magusensis* KCCM40447

Bashu Dev Pardhe [a], Lakshan Paudel [a], So-Ra Han [b], Tae-Jin Oh [a,b,c,*]

[a] *Department of Life Science and Biochemical Engineering, Sun Moon University, Asan, Republic of Korea*
[b] *Genome-based BioIT Convergence Institute, Asan, Republic of Korea*
[c] *Department of Pharmaceutical Engineering and Biotechnology, Sun Moon University, Asan, Republic of Korea*

ARTICLE INFO

Keywords:
Cytochrome P450
Genomic environment
O-demethylation
Electron transfer redox system
4-Methoxybenzoate
Amycolatopsis magusensis KCCM40447

ABSTRACT

Cytochrome P450 monooxygenases perform a multitude of roles, including the generation of hydroxylated aromatic compounds that might be utilized by microorganisms for their survival. WGS data of *Amycolatopsis magusensis* KCCM40447 revealed a complete circular genome of 9,099,986 base pairs and functionally assigned 8601 protein-encoding genes. Genomic analysis confirmed that the gene for 4-methoxybenzoate monoxygenase (CYP199A35) was conserved in close proximity to the gene for 4-hydroxybenzoate transporter (PcaK). The co-localized genes encoding CYP199A35, and ferredoxin-NAD(P) reductase (Mbr) represent a two-component system for electron transfer. CYP199A35 was specific for *O*-demethylation of *para O*-methyl substituted benzoic acid derivatives, 4-methoxybenzoate (4 MB), and 4-methoxycinnamic acid (4MCA) using the native redox partner (Mbr); two-component system and non-physiological redox partners (Pdr/Pdx); three-component system. The catalytic efficiency for *O*-demethylation of 4 MB using Mbr and Pdr/Pdx was 0.02 ± 0.006 min^{-1} μM^{-1} and 0.07 ± 0.02 min^{-1} μM^{-1} respectively. Further, sequence annotation and function prediction by RAST and KEEG analysis revealed a complete catabolic pathway for the utilization of 4 MB by strain KCCM40447, which was also proved experimentally.

1. Introduction

Aromatic compounds represent about 20 % of the earth's biomass and are the primary cause of pollutants obtained from plant decomposition and petroleum waste [1]. The bioremediation of aromatic contaminants is crucial for environmental cleanup. Most microorganisms conserve and acquire metabolic pathways related to the biosynthesis/degradation of aromatic compounds for their adaptation and survival. The well-understood approach for aromatic compound catabolism is studied in aerobic soil bacteria [2]. The phenolic group in natural compounds is highly reactive and usually protected with unreactive methyl ethers. For example, lignin is a heterogeneous aromatic biopolymer rich in aryl methyl ether groups deriving from the precursor's coniferyl and sinapyl alcohol [3]. *O*-demethylation of aromatic compounds before their ring cleavage remains critical for carbon assimilation in natural carbon cycling

* Corresponding author. Department of Life Science and Biochemical Engineering, Sun Moon University, Asan, Republic of Korea.
E-mail addresses: pardhebashu@gmail.com (B.D. Pardhe), lakshanpl88@gmail.com (L. Paudel), 553sora@hanmail.net (S.-R. Han), tjoh3782@sunmoon.ac.kr (T.-J. Oh).

https://doi.org/10.1016/j.heliyon.2024.e25083
Received 6 September 2023; Received in revised form 18 January 2024; Accepted 19 January 2024
Available online 21 January 2024

[4]. *O*-demethylation generates hydroxylated aromatics that might be utilized by the microorganisms for their growth. In addition, these *O*-demethylated compounds may serve as building blocks to produce value-added chemicals through diverse synthetic strategies [5]. The genome analysis can identify the presence of putative genes associated with the catabolism of lignin-derived aromatic compounds including a variety of ring-oxidizing genes, and genes responsible for the catechol and protocatechuate branches of the β-ketoadipate pathway [6,7].

CYP-mediated *O*-demethylation of aromatic compounds was reported earlier [8,9]. Most of the reported bacterial CYP-mediated *O*-demethylase systems include three component systems. CYP199A4 includes ferredoxin (HauPx), and ferredoxin reductase (HaPuR), whereas CYP199A2 includes iron-sulfur (Fe–S) containing ferredoxin, palustrisredoxin (Pux, RPA1872), and Flavin-dependent ferredoxin reductase, palustrisredoxin reductase (PuR, RPA3782 [8–10]. Proteins CYP199A2 and CYP199A4 from *Rhodopseudomonas palustris* strains CGA009 and HaA2 respectively catalyze the hydroxylation of *para*-substituted benzoic acids [10]. Further, a single mutant S244D of CYP199A4 was reported with enhanced activity for a wide range of *para*-methoxy-substituted benzenes [11]. The crystal structures of the (4-methoxybenzoate) 4 MB bound forms of CYP199A2 and CYP199A4 were solved, and the preference for the *para*-substituted substrate for oxidative demethylation was described [12]. In addition, CYP199A25 from *Arthrobacter* sp. was responsible for hydroxylation or demethylation only in the *para* position using the non-physiological redox partners putidaredoxin reductase (Pdr) and putidaredoxin (Pdx) (class I CYP101A1 system of Pseudomonas putida) [13].

The two-component system, including heme iron and non-heme iron monooxygenases, is well-reported for the *O*-demethylation of aromatic compounds. The VanA is a Rieske non-heme iron monooxygenase (ROs), and VanB is a partner reductase that reduces the flavin cofactor by oxidation of NAD(P)H and then transfers the electrons to the Fdx domain, which likely interacts with the VanA and provides electrons necessary for the catalysis. Vanillate demethylase from *Pseudomonas testosteroni* has a broad substrate range and was able to demethylate *m*- and *p*-methoxybenzoate [14] whereas vanillate demethylase from *Pseudomonas fluorescens* and *Acinetobacter* sp. do not prefer *O*-demethylation of *p*-methoxybenzoate [15,16]. All these enzymes were limited with purification and further characterization because their demethylation activity was sensitive to air oxidation. Nishimura and co-workers showed the potential value of *St*VanA–VanB from *Streptomyces* sp. as a whole-cell biocatalyst, but also underlined the major limitations for the exploration of ROs [17]. Later, another group described recombinant co-expression of *Pseudomonas* sp. HR199 VanA and VanB in *Escherichia coli.* The biocatalytic application of demethylation of aromatic substrates at meta position relative to the carboxylic acid moiety and multi-enzyme cascade reactions for effective cofactor regeneration and by-product removal were discovered successfully [7]. A two-component system containing CYP255A (GcoA) and a three-domain reductase (GcoB) from *Amycolatopsis* sp. ATCC 39116 was described in detail as a promiscuous guaiacol *O*-demethylase. This novel arrangement in bacteria where only one redox partner protein, named GcoB, was shown to transfer electrons from NADH to the cytochrome P450 GcoA [6].

Genome analysis can provide comprehensive information regarding the metabolism of compounds, production of secondary metabolites, and bacterial adaptation to xenobiotics. Further, this outlines the core, accessory, and unique genes responsible for particular metabolism in the strains. Considering this knowledge and to find out the complete *O*-demethylation system for 4 MB, we decided to have a deeper look into the 4 MB demethylation system in strain KCCM40447. Here, we highlighted the catabolic pathway for 4 MB from *Amycolatopsis magusensis* KCCM40447. In the present work, we aimed to identify the proteins responsible for 4 MB demethylation with the additional purpose of utilization of 4-hydroxybenzoate (4HB). Here, we illustrated the two-component system including CYP199A35 and its putative redox partner ferredoxin-NAD(P) reductase (Mbr).

2. Materials and methods

2.1. Chemicals and reagents

Benzoic acid derivatives, 4-methoxybenzoate was purchased from Tokyo Chemical Industry Co., Ltd. (Korea), 2-methoxy benzoate, and 3-methoxybenzoate were purchased from Sigma-Aldrich (Korea), 2,5-dimethoxybenzoate, 3,5-dimethoxybenzoate, 2-amino 6-methoxybenzoate, and 4-methoxycinnamic acid (4MCA) were purchased from Biosynth Carbosynth (China). T4 DNA ligase, DNA polymerase, and dNTPs were available from Takara Bio (Japan). α-aminolevulinic acid (ALA), ampicillin (Amp), nicotinamide adenine dinucleotide (NADH), nicotinamide adenine dinucleotide phosphate (NADPH), catalase, formate dehydrogenase, sodium formate, spinach Fdx, and spinach Fdr were obtained from Sigma-Aldrich (Korea). Isopropyl-1-thio-β-D-galactopyranoside (IPTG) and kanamycin (Km) were bought from Duchefa Bohemie (Korea). Restriction enzymes were procured from Takara Clontech (Korea).

2.2. Amycolatopsis magusensis KCCM40447 culture condition and whole genome shotgun (WGS) sequencing

The strain KCCM40447 was purchased from the Korean Culture Centre of Microorganisms (KCCM) in the Republic of Korea. It was cultivated using tryptic soy broth (TSB, BD DIFCO, USA) with agar (MB cell Ltd. Seoul, Republic of Korea). The bacterial culture used for genomic DNA extraction was cultivated at 25 °C for 3 days on TSB. Subsequently, the genomic DNA from strain KCCM40447 was extracted using a QIAamp DNA Mini Kit (Qiagen Inc., Valencia, CA, USA). The quantity and purity of genomic DNA were determined using a spectrophotometer (Biochrome, Libra S35PC, UK). According to the standard protocols, the WGS sequencing of strain KCCM40447 was obtained by the Illumina MiSeq platform (Majorbio, Shanghai). The annotation information was added to the National Center for Biotechnology Information (NCBI) Prokaryotic Genome Annotation Pipeline (PGAP) (https://www.ncbi.nlm.nih.gov/genome/annotation_prok/). The strain KCCM40447 WGS project has been deposited with project accession JASCSI000000000. This project version has the accession number JASCSI010000000 and consists of sequences JASCSI010000001-JASCSI010000817.

2.3. Genome annotation and bioinformatics analysis for sequence prediction

The related whole genome sequences of *Amycolatopsis* species available in GenBank (https://www.ncbi.nlm.nih.gov) were downloaded for identification and comparison with the strain KCCM40447. The whole genome sequence data were analyzed using a free bioinformatics platform for whole genome-based taxonomic analysis at the Type (Strain) Genome Server (TYGS) (https://tygs.dsmz.de) [18]. In addition, the similarity between the strains was confirmed by comparing the values of OrthoANI, which was calculated using an Orthologous Average Nucleotide Identity Tool (OAT) [19]. The WGS sequence of strain KCCM40447 was annotated using the rapid annotation subsystem technology (RAST) server [20]. The functional annotation of genes about separate gene categories, including Clusters of Orthologous Genes (COG) was predicted from the EGGNOG 5.0 [21]. The predicted gene sequences were translated and searched by the NCBI non-redundant database and the Kyoto Encyclopedia of Genes and Genomes (KEGG) database with a cutoff value of 0.01 [22]. A circular map of strain KCCM40447 whole genome was produced using the CGView tool [23]. In addition, we predicted enzyme and enzyme function through multiple sequence alignments that were performed using the program Clustal Omega (version 1.2.4) from EMBL-EBI (https://www.ebi.ac.uk/Tools/msa/clustalo/).

2.4. Utilization of 4-methoxybenzoate by Amycolatopsis magusensis KCCM40447

Amycolatopsis magusensis KCCM40447 was grown in tryptic Soy Broth (TSB) at 25 °C at vigorous shaking. 1 mL seed (OD = 1, 25 °C) culture and 1 mM 4 MB was added in a 250 mL flask containing 50 mL TSB. A flask without 4 MB was considered as a control. In addition, 4-methoxybenzoate utilization and bacterial growth were monitored using minimal media. The minimal media composed of 1.5 g KH_2PO_4, 3.55 g Na_2HPO_4, 0.59 g NH_4Cl, 0.89 g $MgCl_2$, 0.5 mL vitamins solution (10×), 1 mL minerals (10×), and 2.0 g yeast extract were dissolved in 1 L of distilled water and pH adjusted to 7.0 and autoclaved at 121 °C for 15 min. 1 mL seed (OD = 1, 25 °C grown in TSB) culture and 0.5 mM 4 MB was added in a 250 mL flask containing 50 mL minimal media. A flask without 4 MB was used as a negative control and a flask supplemented with additional glucose (0.2 %) was used as a positive control. 1 mL culture was taken to measure the optical density (O.D) and another 1 mL was taken to measure utilization of 4 MB by bacteria at different time intervals (0, 12, 24, 36, and 48 h). The culture was extracted with an equal volume of ethyl acetate, dried, and diluted with 700 μL methanol for quantification by HPLC analysis. The growth absorbance was recorded at 600 nm using Biochrom Libra S35PC UV/visible spectrophotometer (Cambridge, UK).

2.5. Cloning and overexpression of CYPs and redox partners

CYP199A35 (GeneBank: WP_282773100.1) encoding 403 amino acids and native ferredoxin-NAD(P) reductase (Mbr) (GeneBank: WP_282773108.1) encoding 326 amino acids from strain KCCM40447, were amplified by using their specific PCR primers listed in Table S1 in the supplementary information (SI). The purified PCR products were cloned into the pMD20-T vector using *Escherichia coli* XL1-Blue and selected by blue-white screening, and the nucleotide sequences were confirmed by automated sequencing (Macrogen, Korea). Further, CYP199A35 confirmed gene was ligated in pET32a(+), and Mbr confirmed gene was ligated in pET28a(+) and was transformed to *Escherichia coli* XL1-Blue. The construct pET32a-CYP199A35 and pET28a-Mbr were plated on LB agar containing 100 μg/mL ampicillin and kanamycin, respectively. The amplified constructs DNA encoding N-terminal His6-tag protein under the control of a T7 promoter were isolated and transformed into chemically competent C41 (DE3) cells (*E. Coli*) and were plated on LB agar containing 100 μg/mL antibiotics. A 3 mL seed culture was grown for 3 h from a single colony under stress (100 μg/mL antibiotic). 0.3 mL seed culture was added to 100 mL of LB-medium supplemented with 100 μg/mL antibiotics and incubated at an orbital shaker (180 rpm) at 37 °C until cell density was about 0.6 at OD 600 nm. Then, pET32a-CYP199A35 culture was supplemented with 1 mM 5-ALA and 0.5 mM $FeCl_3$ to support heme synthesis. Induction for both constructs was done with 0.4 mM IPTG and was incubated for 72 h at 20 °C for protein synthesis. The cell pellets were harvested by centrifugation (3500 rpm) for 30 min at 4 °C and washed twice with 50 mM potassium phosphate buffer (pH 7.4).

Redox partners Pdr (*camA*) and Pdx (*camB*) were expressed in *Escherichia coli* BL21(DE3) using plasmid constructs pET28a(+) and pET32a(+) as described previously [24]. Cells were harvested by centrifugation (3500 rpm) for 30 min at 4 °C and washed twice with 50 mM potassium phosphate buffer (pH 7.4). Spinach Fdx and Fdr were obtained commercially from Sigma-Aldrich (Korea).

2.6. Purification of CYP and redox partners

Overexpressed cell pellets from CYP199A35, Mbr, Pdx, and Pdr were suspended in a potassium phosphate buffer (pH 7.4) solution and lysed by ultrasonication. The soluble protein-containing fraction was separated by centrifugation at 24,650 g for 20 min at 4 °C and was purified by Ni^{2+} affinity chromatography with the use of the TALON His-tag. Resins-bound proteins were eluted by using elution potassium phosphate buffer (7.4) containing 10 % glycerol, 100 mM NaCl, and different concentration gradients of imidazole (10 mM and 100 mM). The purity of the protein was checked by SDS-PAGE electrophoresis in all the fractions and the purified fraction was concentrated by ultrafiltration with Amicon centrifugal filters with 50 kDa cut-off molecular weight for CYP199A35, 30 kDa molecular weight cut-off for Mbr and Pdr and 10 kDa molecular weight cut-off for Pdx.

2.7. Determination of enzyme concentration

CYP199A35 concentration was determined by CO difference spectra as described previously. The amount of CYP was calculated

from $\varepsilon_{449-489} = 91\ mM^{-1}\ cm^{-1}$ [25]. Pdr concentration was determined as the average of concentrations calculated from wavelengths 378, 454, and 480 nm by using extinction coefficients (ε) of 9.7, 10.0, and 8.5 $mM^{-1}\ cm^{-1}$, respectively [26]. Pdx concentration was also determined as the average of concentrations calculated from wavelengths 415 and 454 nm by using extinction coefficients of 11.1 and 10.4 $mM^{-1}\ cm^{-1}$, respectively [26]. All the samples were scanned using Biochrom Libra S35PC UV/visible spectrophotometer (Cambridge, UK). Mbr concentration was measured using the Bradford method with bovine serum albumin as a standard [27].

2.8. *In vitro* biotransformation

The *in vitro* reactions by CYP199A35 were screened using redox partners (Pdr/Pdx, Fdr/Fdx, and putative Mbr). All the substrates, 4 MB, 2-methoxybenzoate, 2-amino 6-methoxybenzoate, 2,5-dimethoxybenzoate, 3-methoxybenzoate, 3,5-dimethoxybenzoate, and 4MCA were prepared in 100 mM stock in DMSO solvent. All the *in vitro* biotransformation was carried out in a 250 μL reaction mixture of 50 mM phosphate buffer (pH 7.4). The *in vitro* reaction mixture for CYP199A35/Pdr/Pdx system contains (CYP:Pdr:Pdx ratio 1:3:9) 3 μM CYP, 9 μM Pdr, 27 μM Pdx, catalase (100 mg/mL), $MgCl_2$ (1 mM), substrate (400 μM), and NADH regeneration system (1 U formate dehydrogenase and 150 mM sodium formate). Similarly for CYP199A35/Fdr/Fdx system, the reaction was catalyzed with (CYP:Fdr:Fdx ratio 1:2:10) 3 μM CYP, 6 μM Fdr, 30 μM Fdx, catalase (100 mg/mL), $MgCl_2$ (1 mM), substrate (400 μM), and NADPH regeneration system (1 U glucose 6 phosphate dehydrogenase and 10 mM glucose 6 phosphate). CYP199A35/Mbr system was optimized with 3 μM CYP, 39 μg Mbr, 400 μM substrate and, using both NADH/NADPH regeneration systems. Reactions were initiated by NAD(P)H and incubated for 2 h at 30 °C with vigorous shaking at 1000 rpm.

2.9. *Product extraction, purification, and analysis*

The reaction mixtures were extracted using equal volumes of ethyl acetate twice, dried, and dissolved in HPLC-grade methanol for further analysis. The mixture was filtered with 0.2 μm Whatman filter then injected into UHPLC and separated with the use of Mightysil reverse-phase C18 column (4.6 × 250 mm, 5 μm); Kanto Chemical, Tokyo, Japan. The gradient system includes 0.05 % TFA water (A) and acetonitrile (B) as mobile phases for separation. All the samples were analyzed using a gradient of B of 10 % for 0–2 min, 50 % for 2–8 min, 70 % for 8–14 min, 95 % for 14–16 min, and 10 % for 16–25 min at the flow rate of 1 mL/min. Substrates and their hydroxylated products were detected by UV-A at 245 nm.

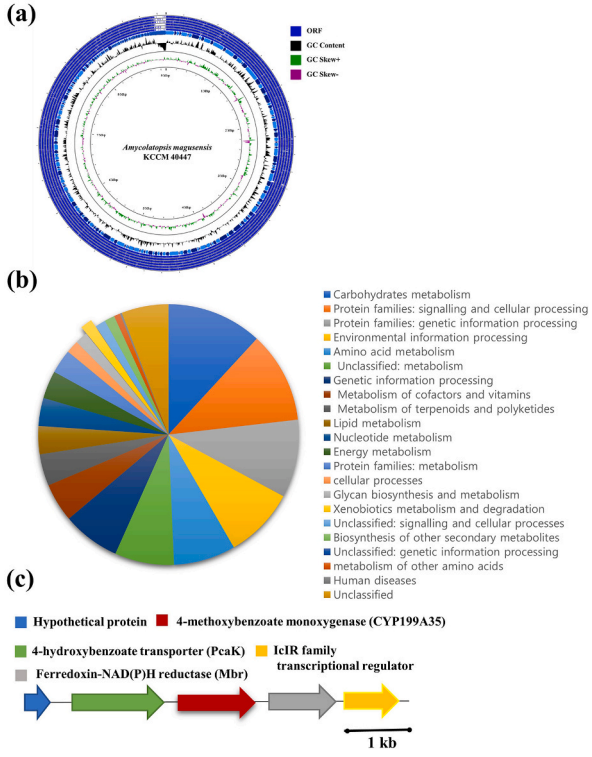

Fig. 1. Genomic analysis of *Amycolatopsis magusensis* KCCM40447. (**a**) Circular genome map of *Amycolatopsis magusensis* KCCM40447. (**b**) An overview of KEGG annotated gene distribution. (**c**) Genomic environment for 4-methoxybenzoate monoxygenase (*O*-demethylating) (CYP199A35).

2.10. Determination of kinetic parameters

The product formation was determined for 1 h using 1 μM CYP, Pdr/Pdx system, and Mbr in the same ratio as mention above with 400 μM substrate in Potassium phosphate buffer pH 7.4 at 30 °C. Kinetics parameter for 4 MB (ranging from 20–800 μM) was analyzed by using CYP199A35, Pdr, and Pdx 1 μM, 3 μM, and 9 μM respectively, and CYP199A35 and Mbr 1 μM, and 13 μM respectively. The conversion (%) of the product was calculated from the area of the product peaks based on the HPLC chromatogram. Assuming the absorbance properties of the product and substrate are the same, the product was quantified by correlating the peak area of the respective product with the combined peak area of the product and the substrate. K_m and k_{cat} values were calculated by plotting the product formation rate against substrate concentration using nonlinear regression analysis, assuming Michaelis-Menten steady-state kinetics.

3. Results and discussion

3.1. Functional annotation of strain KCCM40447 genome

The identification of strain KCCM40447 was verified using whole genome analysis. We compared the subjected genome with the genomes of all type strains database using the MASH algorithm, a fast approximation of relatedness between genomes, and the genome was then matched with the type of strain that exhibited the smallest MASH distance from TYGS [18]. In addition, a pairwise comparison of strains of the same type as KCCM40447 was performed using the genome blast distance phylogeny approach (GBDP), and the exact inter-genome distance could be inferred according to the trimming algorithm and distance (Fig. S1a). Consequently, we compared average nucleotide identity (ANI) values between our strain and seven strains of the closest type lineages determined in the TYGS database with the sequenced genome data. This comparison aimed to assess the ANI values and determine the bacteria species identified between our strain and the selected reference strains. ANI analysis shows the average nucleotide identity of all bacterial orthologous genes classified between two genome sequences. It offers identification between bacterial strains of the same or closely related species (i.e., species showing over 96 % ANI values) [28,29]. In Fig. S1b, the closest ANI value between KCCM40447 and the *Amycolatopsis magusensis* DSM 45510 was 98.82 %, considerably higher than the threshold value of 96 % for the boundary of species circumscription. However, the value was significantly lower than 96 % compared to the rest of the species, so obtaining close results with other species was impossible. Thus, we deposited the strain as *Amycolatopsis magusensis* KCCM40447 to the NCBI database.

As shown in Fig. 1a, the whole genome of strain KCCM40447 comprises 9,099,986 bp with 8747 genes predicted on the chromosome and, 8601 protein-encoding genes were functionally assigned. The remaining genes were predicted as 88 pseudogenes and 58 ribosomal RNA genes. The strain KCCM40447 WGS project has been deposited with the project accession JASCSI000000000 (https://www.ncbi.nlm.nih.gov/nuccore/JASCSI000000000.1/). A total of 22 functional COG categories were classified in this strain. The most numerous COG categories are followed by transcription (category K, 1110 genes), amino acid transport and metabolism (category E, 795 genes), carbohydrate transport and metabolism (category G, 507 genes), energy production and conversion (category C, 479 genes), and except on unknown function genes (category S, 1566) (Fig. S2a). The feature of proteins belonging to specific COG functional categories in a given genome has proven to be a valuable genomic attribute. Consequently, the Genome Standards Consortium has embraced it as a crucial criterion for newly sequenced genomes [30].

The "Metabolism" category in COG encompasses protein functions associated with biological metabolic activities. Therefore, according to the COG annotation results, the predicted features of strain KCCM40447's genome suggest that the "Metabolism" category, specifically category E (amino acid transport and metabolism), category G (carbohydrate transport and metabolism), and category C (energy production and conversion) are predominant. This indicates that the gene content related to the amino acid, carbohydrate, and related energy metabolism is highly conserved in strain KCCM40447. In support, a total of 2866 genes were classified into 22 KEGG functional categories with an abundance of genes assigned to carbohydrates as well as amino acid metabolism (Fig. 1b).

3.2. Genomic insight for 4 MB metabolism

Benzoate degradation genes were predominant in the 'Xenobiotics metabolism and degradation' category from strain KCCM40447 involving a complete catabolic pathway for 4-methoxybenzoate only (Figure S2b and Fig. 2). CYPs belong to this Xenobiotics metabolism category and are primarily associated with diverse metabolic activities such as inheritance transfer, drug metabolism, carbohydrate metabolism, and physiological metabolism in microorganisms [31–34]. Usually, bacteria are essential in the breakdown of polyphenolic compounds, for example, Sphingomonas paucimobilis SYK-6 can degrade lignin-related derivatives via the protocatechuate 4,5-cleavage pathway or multiple 3-*O*-methylgallate catabolic pathways [35]. *O*-demethylation of phenolic compounds before ring cleavage is crucial for their degradation. These reactions are catalyzed by different *O*-demethylase systems in bacteria, such as tetrahydrofolate-dependent *O*-demethylase DesA and LigM from *S. paucimobilis* SYK-6 [36,37] and CYPs [33]. A closer look at the downstream of the gene encoding 4-methoxybenzoate monoxygenase (*O*-demethylating) shows there was the gene encoding for putative ferredoxin-NAD(P) reductase (Mbr) with the same direction in KCCM40447, which might deliver the electrons from NAD(P)H to the monooxygenase (Fig. 1c). The putative gene assigned as 4-hydroxybenzoate transporter (*pcaK*) was upstream to the gene encoding 4-methoxybenzoate monoxygenase. These three genes are sequentially composed in the same direction with a relatively small intergenic gap, indicating that these genes may transcribe under the control of a single promoter. PcaK is localized to the membrane and associated with the transportation of aromatic compounds [38]. It is unlikely that bacterial CYP and putative Fdx-Fdr occur in the periplasm. These kinds of systems along with the likely source of reducing equivalents, typically occur in the cytoplasm. In

this respect, the role of PcaK for the transportation of 4MB/4HB and other lignin derivatives remains the scope for future study [38]. We reasoned that the presence of 4-methoxybenzoate monoxygenase and its redox partner close to PcaK might be dedicated to the *O*-demethylation of 4 MB for the production of 4HB. Analysis of the KCCM40447 genome using RAST annotation and KEGG pathway revealed a predicted pathway for the catabolism of 4HB (Fig. 2 and Table S2). Briefly, 4HB is hydroxylated by 4HB 3-monooxygenase (PobA) to yield protocatechuate, which is converted to central metabolites through the beta-ketoadipate pathway [39].

The function prediction of the 4-methoxybenzoate monoxygenase was further analyzed by phylogenesis and multiple sequences alignment with other homologous enzymes known for the O-demethylation of aromatic compounds [10–13]. The higher identity and conservation at the protein sequence level represent this monoxygenase may be responsible for the *O*-demethylation of different benzoic acid derivatives. Multiple sequence alignment revealed the closest relation with the CYP199A family (Fig. S3). Monoxygenase showed 67 % identity with CYP199A25 from *Arthrobacter* sp., 55.7 % with CYP199A2, and 53.6 % with CYP199A4 from *Rhodopseudomonas palustris,* and 52.4 % identity with CYP199A1 from *Bradyrhizobium japonicum* (Table 1). Further, 4-methoxybenzoate monoxygenase from strain KCCM40447 was assigned the name CYP199A35 using the approved CYP nomenclature (David R. Nelson, Univ. of Tennessee) (https://drnelson.uthsc.edu/CytochromeP450.html). Most of the bacterial CYPs are type I class (three--component system) and require Fdx and Fdr, which transfer electrons from reducing equivalents (NAD(P)H) to the cytochrome [31]. The co-localized genes encoding CYP199A35 and putative Mbr may represent the type II class (two-component system) in strain KCCM40447. Further, conserved domains of Mbr were analyzed. It possesses a 2Fe–2S iron-sulfur cluster binding domain, similar to phthalate dioxygenase reductase (PDR) and vanillate *O*-demethylase oxidoreductase (VanB). The 326 amino acids length protein shows PDR_like, FMN-dependent oxidoreductase from 22 to 228 while it showed fer2 cluster binding domain from 242 to 320. We speculated this PDR/VanB family oxidoreductase is involved in electron transfer from NAD(P)H to CYP199A35. Recently, the

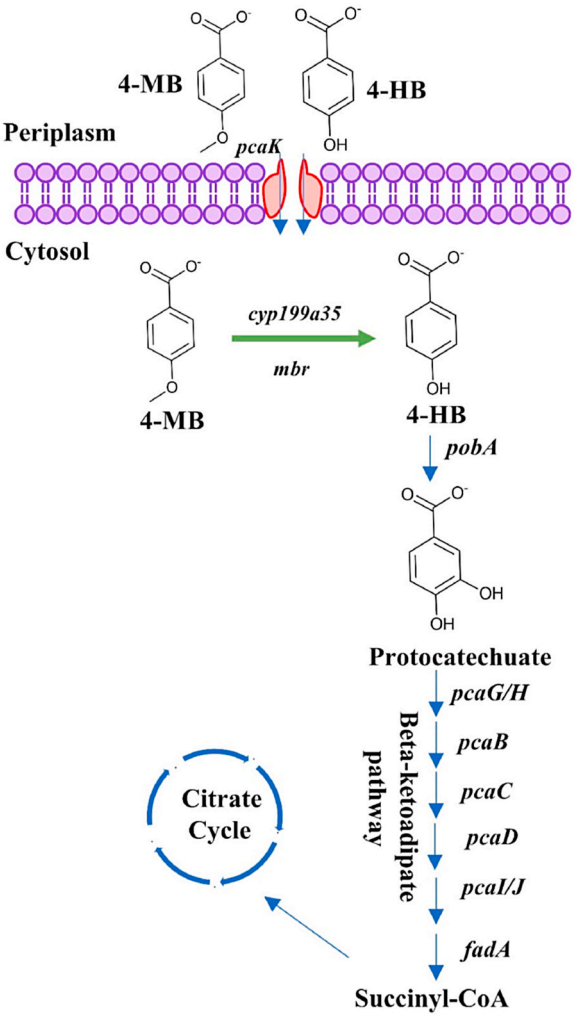

Fig. 2. The proposed catabolic pathway for utilization of 4 MB by *Amycolatopsis magusensis* KCCM40447. All the functional genes were predicted by RAST annotation. The green arrow represents the experimentally characterized pathway in this study. Table S2 shows detailed information about all the genes. (For interpretation of the references to colour in this figure legend, the reader is referred to the Web version of this article.)

Table 1
Homologous proteins of CYP199A35 from the CYP199A subfamily.

% Identity	CYP199A1, BAC46313.1 (*Bradyrhizobium japonicum*)	CYP199A2, WP_011157377.1 (*Rhodopseudomonas palustris*)	CYP199A4, 5KDB_A (*Rhodopseudomonas palustris*)	CYP199A25, WP_091467048 (*Arthrobacter* sp.)
CYP199A35, WP_282773100.1 (*Amycolatopsis magusensis* KCCM40447)	52.40	55.70	53.67	67.00

two-component P450 class representing aromatic *O*-demethylase for lignin bioconversion was identified as GcoAB from strain ATCC39116. Here also, GcoB was responsible for electron transfer from NADH to GcoA, which possesses an N-terminal 2Fe–2S domain and a C-terminal region consisting of a FAD-binding domain homology to FAD-type cytochrome P450 reductase [6]. This highlights the convergence of two-component systems for these special monooxygenases for specific functions in bacteria.

3.3. Utilization of 4 MB by KCCM40447

To further confirm whether the putative 4 MB degradation pathway in KCCM40447 was functional, the strain was supplemented with 1 mM 4 MB and was grown in TSB. The result showed that the exogenous addition of 1 mM 4 MB had a positive effect on growth. The 4 MB level in the culture was decreased by one-third in 24 h and a very low level was detected after 36 h (Fig. 3a). This indicates that KCCM40447 can utilize 4 MB even in rich media (TSB). In addition, the growth of KCCM40447 on 0.5 mM 4 MB supplementation was tested using minimal media. Growth was observed and about 95% of 4 MB was utilized by the strain in 48 h (Fig. 3b). 4 MB is distributed in plant and lignin and are associated with microorganism for its mineralization [32]. The regulation of aromatic compounds catabolism is secondary to carbohydrates and several unique regulatory features in the 4HBA degradation mechanism have been presented [39,40]. KCCM40447 also possesses all the responsible genes for the complete degradation of 4 MB and 4HB. We opened for the detailed study of operon organization, and regulatory genes that control the expression of key enzymes for the purpose

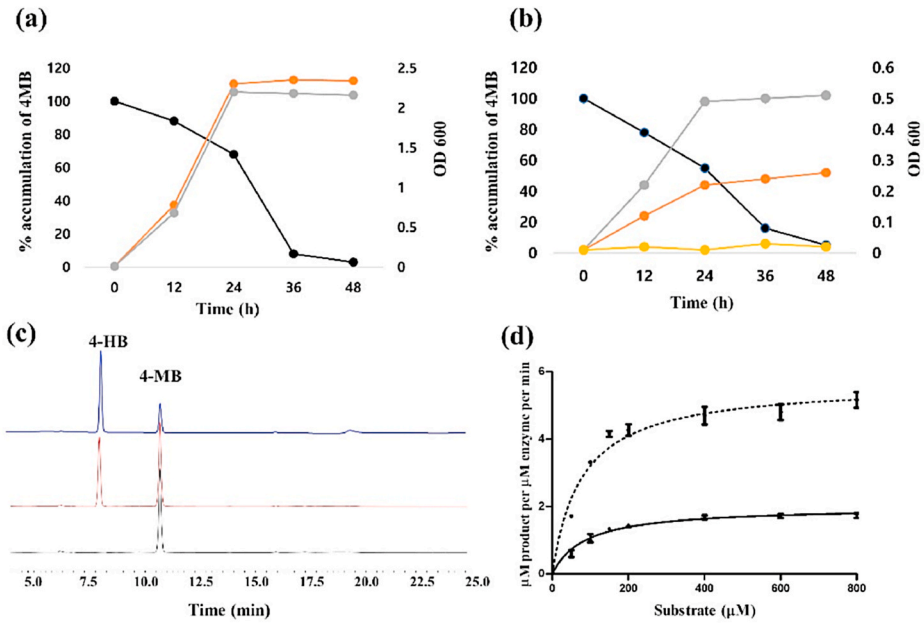

Fig. 3. (**a**) Growth and utilization of 4 MB by *Amycolatopsis magusensis* KCCM40447 in TSB. Growth pattern for control (grey) and 1 mM 4 MB supplemented (orange) and utilization pattern (black) for 4 MB. (**b**) Growth and utilization of 4 MB by *Amycolatopsis magusensis* KCCM40447 in minimal media. Growth pattern for the positive control (grey), negative control (yellow), and 0.5 mM 4 MB supplemented (orange), and utilization pattern (black) for 4 MB (**c**) HPLC analysis for CYP199A35 mediated *O*-demethylation of 4 MB. Chromatogram (blue) represents product formation by a CYP199A35-Pdr/Pdx system, and chromatogram (red) represents product formation by the CYP199A35-Mbr system, and chromatogram (black) represents negative control with boiled enzymes. (**d**) Hyperbolic fit for the *O*-demethylation of 4 MB to 4HB catalyzed by CYP199A35. The dotted line indicates the reaction catalyzed by a three-component reaction system including CYP199A35-Pdr/Pdx. The reaction rate was calculated from an initial 20 min reaction in potassium phosphate buffer pH 7.4 using 1 µM CYP, 3 µM Pdr, and 9 µM Pdx at 30 °C. The continuous line represents the reaction catalyzed by a two-component reaction system including CYP199A35-Mbr. The reaction rate was calculated from an initial 20 min reaction in potassium phosphate buffer pH 7.4 using 1 µM CYP, and 13 µM Mbr at 30 °C. Mean ± standard deviations were calculated from the three independent experiments. (For interpretation of the references to colour in this figure legend, the reader is referred to the Web version of this article.)

and mechanism of 4 MB utilization by KCCM40447.

3.4. Substrate spectrum and selectivity of CYP199A35

CYP199A35, co-localized putative Mbr, Pdr, and Pdx (class I CYP101A1 system of Pseudomonas putida) were cloned and over-expressed, and soluble proteins were purified. The purified single band of CYP199A35 was obtained and characterized by a CO-reduction assay. The purified enzyme had an Rz value of 1.45, thus indicating high purity. The theoretical molecular weight for CYP199A35 and putative Mbr were 44.2 kDa and 35 kDa, respectively. The SDS_PAGE analysis showed a band at ≈62 kDa for CYP199A35 (Trx-His-*s*-enterokinase fusion sequence translated from pET32a(+)) and ≈44 kDa band for Mbr (fusion sequence translated from pET28a(+)) (Fig. S4 and Fig. S5 in SI). As predicted, the gene cluster was dedicated to the production of 4HB, we selected substrate 4 MB for the *O*-demethylation by CYP199A35. In addition, to observe the substrate selectivity by CYP199A35, different methoxy-benzoic acid derivatives listed in Scheme 1 were screened. 2-methoxybenzoate, 3-methoxybenzoate, 2,5-dimethoxybenzoate, 3,5-dimethoxybenzoate, 2-amino 6-methoxybenzoate and 4MCA were screened for *in vitro* biotransformation by CYP199A35 using Pdr/Pdx system, Fdx/Fdr (commercial), and putative Mbr as redox partners. Notably, CYP199A35 was specific to *O*-demethylation of *para O*-methyl substituted benzoic acid derivatives, 4 MB and 4MCA. 4 MB and 4MCA were efficiently *O*-demethylated to 4HB and 4-hydroxycinnamic acid (4HCA), respectively by CYP199A35 using the native two-component system, Mbr and three-component system of non-physiological redox partners (Pdr/Pdx system). The retention time (R_t) for products 4HB (8.4 min) and 4HCA (9.6 min) was confirmed by comparing the standard compounds in the HPLC chromatogram (Fig. 3c and Fig. S6). Recently reported, class I systems CYP199A2-Pux-PuR from *Rhodopseudomonas palustris* CGA009, and CYP199A4-HaPux-HaPuR from *Rhodopseudomonas palustris* HaA2 were capable of the *O*-demethylation of 4 MB using their native redox partners [10,41]. Interestingly, CYP199A35 supports a class I system (Pdr/Pdx) and a two-component system (Mbr) for electron transport from the co-factor NADH. Native redox partners are not always closely associated with the CYP in the gene cluster like HaPux-HaPuR are not associated with CYP199A4, but they work together efficiently [10,11]. Here we provide the advantage of genome mining and evaluating the associated gene with the CYP for substrate selection and specific metabolic function in bacteria.

Finally, the steady-state kinetic parameters of CYP199A35 were determined. Initial velocity was measured with 1 μM CYP for 20 min after knowing the time-dependent conversion course by the enzyme (Fig. S7). *O*-demethylation of 4 MB by CYP199A35 by using Mbr and Pdr/Pdx system was investigated (Fig. 3d). K_m and k_{cat} values for *O*-demethylation of 4 MB by different CYP199A subfamilies using different electron transfer systems are listed in Table 2. The catalytic efficiency (k_{cat}/K_m) for *O*-demethylation of 4 MB using Mbr and Pdr/Pdx was 0.02 ± 0.006 min^{-1} μM^{-1} and 0.07 ± 0.02 min^{-1} μM^{-1}, respectively. Even though the genomic environment for 4 MB catabolism in strain KCCM40447 shows the real redox partner for CYP199A35 was Mbr, it supports the non-physiological partners (Pdr/Pdx) with ≈3.5-fold with higher catalytic efficiency and no activity with Fdr/Fdx system. This indicates that the bacterial CYPs have different compatibility with the different redox partners for efficient catalysis. Besides the genomic organization, P450-redox partner interactions also modulate the catalytic activity [42]. On the other aspects, the use of large tags to purify the Mbr may interfere with the interaction with CYP199A35 and diminish the activity. CYP199A2 supports its native redox partner palustrisredoxin (Pux) in combination with Pdr from *Pseudomonas putida* for substrate oxidation [43]. Previously, CYP199A25 from *Arthrobacter* sp. was analyzed for the compatibility of redox partners with different combinations. They also achieve higher product formation using the non-physiological redox partners, Pdr/Pdx like CYP199A35 [13]. This suggests the mining of physiological redox partners and the use of heterologous partners remains important when the biological importance of the CYP199A subfamily is envisioned. Recognition of the physiological electron transfer system of CYPs also leads to new insights into the evolution of this important family of proteins [44]. In addition, solving the crystal structure and further engineering can provide insight into their substrate specificity. Structural analysis and mutagenesis of CYP199A4 from the same subfamily highlights the involvement of F185, R92, S95, and R243 residues in the binding and catalysis of para-substituted benzoate derivatives [12]. Mutagenesis on single active site residue F185 of CYP199A4 provides the rationale for the selectivity of product oxidation, converting the enzyme into 4-ethylbenzoic acid desaturase [45]. Further, solving the crystal structure of CYP199A35, identification of substrate binding residues, and their mutagenesis can expand the substrate scope.

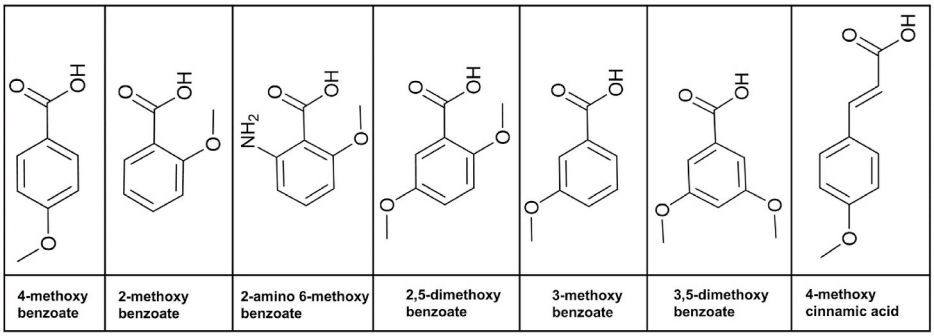

Scheme 1. Benzoic acid derivatives used for screening CYP199A35.

Table 2
Comparison of kinetic parameters for *O*-demethylation of 4 MB by different CYPs and their redox partners combination.

CYPs [Reference]	Redox system	K_m (μM)	k_{cat} (min^{-1})	k_{cat}/K_m (min^{-1} μM^{-1})	In vitro conversion (%)
CYP199A35 [This study]	Pdr/Pdx	80 ± 10	5.7 ± 0.2	0.07 ± 0.02	97 ± 2
CYP199A35 [This study]	Mbr	90 ± 15	2.1 ± 0.1	0.02 ± 0.006	43 ± 2
CYP199A25 [13]	Pdr/Pdx	46.5 ± 2.2	3.36 ± 0.05	0.07 ± 0.02 [b]	63.2 ± 1.8
CYP199A2 [10]	PuR/Pux	0.45 ± 0.04	2274 ± 48 [a]	5053 ± 1200 [b]	–
CYP199A2 [10]	HaPuR/HaPux	0.53 ± 0.1	2904 ± 114 [a]	5479 ± 1140 [b]	–
CYP199A4 [10]	HaPuR/HaPux	1.41 ± 0.1	2556 ± 48 [a]	1813 ± 480 [b]	–

Mean ± standard deviation was calculated from the three independent experiments in this study, [a] k_{cat} values provided Sec^{-1} in the literature were converted to min^{-1}, [b] Values were not provided in the literature, calculative values are presented for comparison.

4. Conclusions

In this study, we performed genome sequencing of *Amycolatopsis magusensis* KCCM40447. COG analysis revealed that the gene content related to the amino acid, carbohydrate, and related energy metabolism is highly conserved in strain KCCM40447. Benzoate degradation genes were predominant in the Xenobiotics metabolism category. Further querying the genome, we found that the putative CYP encoding gene was conserved close to the putative 4HB transporter (*pcaK*). CYP encoding gene was co-localized with the gene encoding for putative Fdx-Fdr. CYP199A35 and its redox partner (Mbr) were investigated with bioinformatics analysis, then cloned and overexpressed. CYP199A35 was dedicated to the O-demethylation of 4 MB with its physiological redox partner (Mbr) and non-physiological redox partner (Pdx/Pdr). Further, the catabolic pathway for 4HB, produced by a two-component system (CYP199A35-Mbr) from 4 MB was predicted by RAST and KEGG analysis. Strain KCCM40447 holds the genomic information for the catabolism of 4 MB, which may be the significance for energy metabolism and bioremediation of aromatic pollutants by microorganisms.

Data availability statement

Data are available on reasonable request. All the data are available in manuscript and supplemetary document. The strain KCCM40447 WGS project has been deposited with the project accession JASCSI000000000 in NCBI database (https://www.ncbi.nlm.nih.gov/nuccore/JASCSI000000000.1/).

CRediT authorship contribution statement

Bashu Dev Pardhe: Writing – review & editing, Writing – original draft, Resources, Methodology, Investigation, Conceptualization. **Lakshan Paudel:** Writing – review & editing, Writing – original draft, Methodology, Investigation. **So-Ra Han:** Writing – review & editing, Writing – original draft, Methodology, Investigation. **Tae-Jin Oh:** Writing – review & editing, Writing – original draft, Visualization, Validation, Supervision, Methodology, Investigation, Conceptualization.

Declaration of competing interest

The authors declare that they have no known competing financial interests or personal relationships that could have appeared to influence the work reported in this paper.

Acknowledgments

This work was supported by the Technology Innovation Program (20018705, Development of masking and commercialization of biodegradable technology in an urban residential environment using rancid odor-reducing microorganisms and its fragrances) funded by the Ministry of Trade, Industry & Energy (MOTIE, Korea). This research was also supported by a project entitled “Development of potential antibiotic compounds using polar organism resources (20200610)” funded by the Ministry of Oceans and Fisheries, Republic of Korea.

Appendix B. Supplementary data

Supplementary data to this article can be found online at https://doi.org/10.1016/j.heliyon.2024.e25083.

References

[1] E. Díaz, J.I. Jiménez, J. Nogales, Aerobic degradation of aromatic compounds, Curr. Opin. Biotechnol. 24 (3) (2013) 431–442.
[2] G. Fuchs, M. Boll, J. Heider, Microbial degradation of aromatic compounds-From one strategy to four, Nat. Rev. Microbiol. 9 (11) (2011) 803–816.

[3] G. de Gonzalo, D.I. Colpa, M.H.M. Habib, M.W. Fraaije, Bacterial enzymes involved in lignin degradation, J. Biotechnol. 236 (2016) 110–119.
[4] S.J. Mallinson, M.M. Machovina, R.L. Silveira, M. Garcia-Borràs, N. Gallup, C.W. Johnson, et al., A promiscuous cytochrome P450 aromatic *O*-demethylase for lignin bioconversion, Nat. Commun. 9 (1) (2018) 2487.
[5] E. Lanfranchi, M. Trajković, K. Barta, J.G. de Vries, D.B. Janssen, Exploring the selective demethylation of aryl methyl ethers with a *Pseudomonas Rieske* monooxygenase, Chembiochem 20 (1) (2019) 118–125.
[6] C.S. Harwood, R.E. Parales, The β-ketoadipate pathway and the biology of self-identity, Annu. Rev. Microbiol. 50 (1) (1996) 553–590.
[7] G. Janusz, A. Pawlik, J. Sulej, U. Świderska-Burek, A. Jarosz-Wilkołazka, A. Paszczyński, Lignin degradation: microorganisms, enzymes involved, genomes analysis and evolution, FEMS Microbiol. Rev. 41 (6) (2017) 941–962.
[8] A. Dardas, D. Gal, M. Barrelle, G. Sauret-Ignazi, R. Sterjiades, J. Pelmont, The demethylation of guaiacol by a new bacterial cytochrome P-450, Arch. Biochem. Biophys. 236 (2) (1985) 585–592.
[9] L.D. Eltis, U. Karlson, K.N. Timmis, Purification and characterization of cytochrome P450RR1 from *Rhodococcus rhodochrous*, Eur. J. Biochem. 213 (1) (1993) 211–216.
[10] S.G. Bell, A.B.H. Tan, E.O.D. Johnson, L.L. Wong, Selective oxidative demethylation of veratric acid to vanillic acid by CYP199A4 from *Rhodopseudomonas palustris* HaA2, Mol. Biosyst. 6 (1) (2009) 206–214.
[11] R.R. Chao, I.C.K. Lau, J.J. De Voss, S.G. Bell, Modification of an enzyme biocatalyst for the efficient and selective oxidative demethylation of para-substituted benzene derivatives, ChemCatChem 8 (23) (2016) 3626–3635.
[12] S.G. Bell, W. Yang, A.B. Tan, R. Zhou, E.O. Johnson, A. Zhang, et al., The crystal structures of 4-methoxybenzoate bound CYP199A2 and CYP199A4: Structural changes on substrate binding and the identification of an anion binding site, Dalt Trans 41 (28) (2012) 8703–8714.
[13] J.M. Klenk, J. Ertl, L. Rapp, M.P. Fischer, B. Hauer, Expression and characterization of the benzoic acid hydroxylase CYP199A25 from *Arthrobacter* sp, Mol. Catal. 484 (2020) 110739.
[14] D.W. Ribbons, Requirement of two protein fractions for *O*-demethylase activity in *Pseudomonas testosteroni*, FEBS Lett. 12 (3) (1971) 161–165.
[15] B. Morawski, A. Segura, L.N. Ornston, Substrate range and genetic analysis of *Acinetobacter* vanillate demethylase, J. Bacteriol. 182 (5) (2000) 1383–1389.
[16] N.J. Cartwright, A.R.W. Smith, Bacterial attack on phenolic ethers: an enzyme system demethylating vanillic acid, Biochem. J. 102 (3) (1967) 826–841.
[17] M. Nishimura, Y. Nishimura, C. Abe, M. Kohhata, Expression and substrate range of *Streptomyces* vanillate demethylase, Biol. Pharm. Bull. 37 (9) (2014) 1564–1568.
[18] J.P. Meier-Kolthoff, M. Göker, TYGS is an automated high-throughput platform for state-of-the-art genome-based taxonomy, Nat. Commun. 10 (1) (2019) 2182.
[19] I. Lee, Y. Ouk Kim, S.C. Park, J. Chun, OrthoANI: an improved algorithm and software for calculating average nucleotide identity, Int. J. Syst. Evol. Microbiol. 66 (2) (2016) 1100–1103.
[20] R.K. Aziz, D. Bartels, A.A. Best, M. DeJongh, T. Disz, R.A. Edwards, et al., The RAST Server: rapid annotations using subsystems technology, BMC Genom. 9 (1) (2008) 1–5.
[21] C.P. Cantalapiedra, A. Hernández-Plaza, I. Letunic, P. Bork, J. Huerta-Cepas, eggNOG-mapper v2: functional annotation, orthology assignments, and domain prediction at the metagenomic scale, Mol. Biol. Evol. 38 (12) (2021) 5825–5829.
[22] M. Kanehisa, S. Goto, KEGG: Kyoto Encyclopedia of genes and genomes, Nucleic Acids Res. 28 (1) (2000) 27–30.
[23] J.R. Grant, A.S. Arantes, P. Stothard, Comparing thousands of circular genomes using the CGView Comparison Tool, BMC Genom. 13 (1) (2012) 1–8.
[24] S. Bhattarai, K. Liou, T.J. Oh, Hydroxylation of long chain fatty acids by CYP147F1, a new cytochrome P450 subfamily protein from *Streptomyces peucetius*, Arch. Biochem. Biophys. 539 (1) (2013) 63–69.
[25] T. Omura, R. Sato, The Carbon monoxide-binding pigment of liver microsomes. I. Evidence for its hemoprotein nature, J. Biol. Chem. 239 (7) (1964) 2370–2378.
[26] M.M. Purdy, L.S. Koo, P.R. Ortiz De Montellano, J.P. Klinman, Steady-state kinetic investigation of cytochrome P450cam: interaction with redox partners and reaction with molecular oxygen, Biochemistry 43 (1) (2004) 271–281.
[27] M.M. Bradford, M.M. Bradford, A rapid and sensitive mocrogram quantities of protein utilizing the priciple of protein dye biding, Anal. Biochem. 72 (1–2) (1976) 248–254.
[28] J. Goris, K.T. Konstantinidis, J.A. Klappenbach, T. Coenye, P. Vandamme, J.M. Tiedje, DNA–DNA hybridization values and their relationship to whole-genome sequence similarities, Int. J. Syst. Evol. Microbiol. 57 (1) (2007) 81–91.
[29] M. Richter, R. Rosselló-Móra, Shifting the genomic gold standard for the prokaryotic species definition, Proc. Natl. Acad. Sci. USA 106 (45) (2009) 19126–19131.
[30] M.Y. Galperin, D.M. Kristensen, K.S. Makarova, Y.I. Wolf, E.V. Koonin, Microbial genome analysis: the COG approach, Brief Bioinform 20 (4) (2019) 1063–1070.
[31] R. Bernhardt, Cytochromes P450 as versatile biocatalysts, J. Biotechnol. 124 (1) (2006) 128–145.
[32] A. Greule, J.E. Stok, J.J. De Voss, M.J. Cryle, Unrivalled diversity: the many roles and reactions of bacterial cytochromes P450 in secondary metabolism, Nat. Prod. Rep. 35 (8) (2018) 757–791.
[33] M.E. Wolf, D.J. Hinchen, J.L. DuBois, J.E. McGeehan, L.D. Eltis, Cytochromes P450 in the biocatalytic valorization of lignin, Curr. Opin. Biotechnol. 73 (2022) 43–50.
[34] L. Reisky, H.C. Büchsenschütz, J. Engel, T. Song, T. Schweder, J.H. Hehemann, et al., Oxidative demethylation of algal carbohydrates by cytochrome P450 monooxygenases, Nat. Chem. Biol. 14 (4) (2018) 342–344.
[35] E. Masai, Y. Katayama, M. Fukuda, Genetic and biochemical investigations on bacterial catabolic pathways for lignin-derived aromatic compounds, Biosci. Biotechnol. Biochem. 71 (1) (2007) 1–15.
[36] E. Masai, M. Sasaki, Y. Minakawa, T. Abe, T. Sonoki, K. Miyauchi, et al., A novel tetrahydrofolate-dependent *O*-demethylase gene is essential for growth of *Sphingomonas paucimobilis* SYK-6 with syringate, J. Bacteriol. 186 (9) (2004) 2757–2765.
[37] T. Abe, E. Masai, K. Miyauchi, Y. Katayama, M. Fukuda, A tetrahydrofolate-dependent *O*-demethylase, LigM, is crucial for catabolism of vanillate and syringate in *Sphingomonas paucimobilis* SYK-6, J. Bacteriol. 187 (6) (2005) 2030–2037.
[38] N.N. Nichols, C.S. Harwood, PcaK, a high-affinity permease for the aromatic compounds 4-hydroxybenzoate and protocatechuate from Pseudomonas putida, J. Bacteriol. 179 (16) (1997) 5056–5061.
[39] N. Ghimire, B. Kim, C.M. Lee, T.J. Oh, Comparative genome analysis among *Variovorax* species and genome guided aromatic compound degradation analysis emphasizing 4-hydroxybenzoate degradation in *Variovorax* sp. PAMC26660, BMC Genom. 23 (1) (2022) 375.
[40] J.Y. Wang, L. Zhou, B. Chen, S. Sun, W. Zhang, M. Li, et al., A functional 4-hydroxybenzoate degradation pathway in the phytopathogen *Xanthomonas campestris* is required for full pathogenicity, Sci Reports 5 (1) (2015) 18456.
[41] S.G. Bell, F. Xu, E.O. Johnson, I.M. Forward, M. Bartlam, Z. Rao, et al., Protein recognition in ferredoxin–P450 electron transfer in the class I CYP199A2 system from *Rhodopseudomonas palustris*, J Biol Inorg Chem 15 (3) (2010) 315–328.
[42] X. Liu, F. Li, T. Sun, J. Guo, X. Zhang, X. Zheng, et al., Three pairs of surrogate redox partners comparison for class I cytochrome P450 enzyme activity reconstitution, Commun. Biol. 5 (1) (2022) 791.
[43] S.G. Bell, F. Xu, I. Forward, M. Bartlam, Z. Rao, L.L. Wong, Crystal structure of CYP199A2, a para-substituted benzoic acid oxidizing cytochrome P450 from *Rhodopseudomonas palustris*, J. Mol. Biol. 383 (3) (2008) 561–574.
[44] F. Hannemann, A. Bichet, K.M. Ewen, R. Bernhardt, Cytochrome P450 systems-biological variations of electron transport chains, Biochim Biophys Acta - Gen Subj 1770 (3) (2007) 330–344.
[45] S.G. Bell, R. Zhou, W. Yang, A.B. Tan, A.S. Gentleman, L.L. Wong, W. Zhou, Investigation of the substrate range of CYP199A4: modification of the partition between hydroxylation and desaturation activities by substrate and protein engineering, Chem.–Eur. J. 18 (52) (2012) 16677–16688.